Mechanistic Modeling of Polymer Pyrolysis: Polypropylene

Todd M. Kruse, Hsi-Wu Wong, and Linda J. Broadbelt*

Department of Chemical Engineering, Northwestern University, Evanston, Illinois 60208

Received June 11, 2003; Revised Manuscript Received September 30, 2003

ABSTRACT: The pyrolysis of polypropylene was modeled at the mechanistic level to predict the formation of low molecular weight products. Differential equations were developed that describe the evolution of the moments of structurally distinct polymer species. Unique polymer groups were devised that allowed the necessary polymeric features for capturing the pyrolysis chemistry to be tracked, while maintaining a manageable model size. The conversion among the species was described using typical free radical reaction types, including intermolecular hydrogen abstraction, midchain β-scission, end-chain β-scission, intramolecular hydrogen transfer, radical addition, bond fission, radical recombination, and disproportionation. The model included over 24 000 reactions and tracked 213 species (27 products tracked with molecular weights below 215 amu). The intrinsic kinetic parameters (a frequency factor and activation energy for each reaction) were obtained from data in the literature and previous modeling work in our laboratory.[1,2] The model predictions for the evolution of the yields of five major alkenes and five major alkanes compare well with experimental data obtained in our laboratory for the pyrolysis of polypropylene over a temperature range of 350−420 °C. In addition, literature data[3] for the evolution of the polypropylene molecular weight was captured by incorporating weak backbone links modeled as peroxide bonds.

Introduction

In recent years, emphasis has been placed on developing techniques to recycle municipal solid waste (MSW). The amount of MSW generated in the United States each year continues to increase, where each person in the United States generated 4.6 lbs of waste per day in 2000, an increase from 2.7 lbs per person per day in 1960.[4] Due to this focus on recycling MSW, some success has been achieved as evidenced by an increase in the amount of MSW recycled from 1999 (16.4%) to 2000 (23%). This increase is larger than the 0.3% increase in the total amount of MSW generated from 1999 to 2000.[4] However, even with this increase in the amount of MSW recycled, the amount recycled of some components of MSW is significantly lagging behind that of other components. One segment of MSW that is of concern is plastic waste, where plastics comprise 10.7 wt % (>30 vol %) of municipal solid waste, and only 5.4% of plastic waste was recycled in the United States in 2000.[4] Adding to the concern, plastics are considered to be one of the most rapidly growing segments of municipal solid waste,[4] and for some types of plastic waste, the amount recycled is near zero. For instance, 13.6 wt % of plastic waste was composed of polypropylene in the United States in 2000, and only about 0.3% of this polypropylene was recycled.[4]

Several options exist for recycling waste plastic, and these options can be lumped into the following four categories:[5] (1) reusing waste plastic products directly for other applications; (2) reprocessing waste plastic into secondary products; (3) recovering valuable chemical resources from waste plastic; and (4) incinerating waste plastic to recover energy. The resource recovery strategy (category 3 above) involves converting polymers into fuels and chemicals and recovering monomer to produce new polymer.[6] In our lab, the thermal technique of pyrolysis was investigated as a resource recovery strategy. Pyrolysis is an attractive resource recovery process due to its simplicity, where plastic waste is thermally degraded in the absence of oxygen. In addition, the pyrolysis of polymeric materials has grown as a resource recovery strategy in recent years[7−9] and has a high potential for growth in the coming years provided that economically feasible processes can be developed.[10]

The main obstacles that have prevented the successful implementation of a resource recovery process based on pyrolysis are the lack of a comprehensive understanding of the complex underlying reaction pathways and the difficulty in predicting the full product distribution of pyrolytic degradation. For example, the pyrolysis of polypropylene results in a very diverse product distribution due to the high temperatures used and the complex free radical reactions involved. To overcome these obstacles, population balance based models have been developed using the method of moments to model molecular weight changes and small molecule evolution simultaneously.[11−20] In our previous work,[2,21] these approaches for modeling polymer degradation and polymerization were combined and extended to develop a detailed mechanistic model for polymer pyrolysis. In development of this polymer pyrolysis model, a balance was struck between a fully speciated model and one that does not possess sufficient detail to either capture the experimental measures of interest or differentiate the reactivities of chains with different structural features.

Our previous work concentrated on developing the necessary framework for mechanistic modeling of the decomposition of polymers during pyrolysis by focusing on the pyrolysis of polystyrene,[2,21] and we have now extended this modeling work to investigate the pyrolysis of polypropylene. Detailed information about the decomposition of polypropylene was obtained from experiments in our laboratory, including work reported previously.[22] The yields of specific low molecular weight products as a function of time were measured for polypropylene pyrolysis in a batch reactor. The pyrolysis of polypropylene at different temperatures (350, 380, and 420 °C) was examined.

* To whom correspondence should be addressed: phone, 847-491-5351; fax, 847-491-3728; e-mail, broadbelt@northwestern.edu.

10.1021/ma030322y CCC: $25.00
Published on Web 11/20/2003

The pyrolysis of polypropylene has been studied at different levels of detail in the literature. Overall, the major products from polypropylene pyrolysis were determined to be as follows (in decreasing order): 2,4-dimethyl-1-heptene (trimer), *n*-pentane, 2-methyl-1-pentene (dimer), and propylene.[23] Tsuchiya and Sumi proposed a free radical mechanism analogous to the mechanism for polystyrene pyrolysis (see Kruse et al. 2002) to account for the formation of these products.[23] While the reactions proposed are similar for polystyrene and polypropylene, their relative contributions are dependent on the backbone structure. For example, it has been postulated that hydrogen abstraction occurs more readily in polypropylene due to less steric hindrance compared to polystyrene which has bulky phenyl substituent groups.[24] The reduction in steric hindrance due to the presence of methyl substituent groups results in more hydrogen abstraction, leading to more oligomeric products. Other recent studies have examined the possible presence of weak links within polypropylene chains.[3] It was proposed that peroxide groups exist within polypropylene, but no weak links were detected using Fourier transform infrared spectroscopy (FTIR).[3]

More recent work has analyzed the pyrolysis of polypropylene at temperatures between 500 and 900 °C.[25] Compared to lower temperature studies, a greater conversion to products volatile at room temperature was achieved. In addition, yields of propylene as high as 38% were obtained. Trimer was the product formed in the highest yield. The product distribution was proposed to be most significantly influenced by the occurrence of backbiting reactions (intramolecular hydrogen abstraction by end-chain radicals). The backbiting reaction to the carbon in the fifth position along the backbone leads to the production of trimer and *n*-pentane. However, it was also proposed that intramolecular hydrogen abstraction to the third, seventh, and ninth carbon positions is important during polypropylene pyrolysis, compared to just the third and fifth positions for polystyrene. This postulate was supported by the significant yields of tetramer (2,4,6-trimethyl-1-nonene) and pentamer (2,4,6,8-tetramethyl-1-undecene) which would be evolved from specific radicals at the seventh and ninth carbon positions, respectively. Similar to other studies, the authors proposed that backbiting reactions during polypropylene pyrolysis are more important and diverse than those that occur during polystyrene pyrolysis because of the greater flexibility of polypropylene due to the small methyl substituent groups.

Up to this point, modeling studies in the literature have focused on either obtaining apparent rate parameters for the overall decomposition of polypropylene[26,27] or fitting an effective rate constant to model the polypropylene molecular weight distribution.[28] The primary challenge in modeling polypropylene pyrolysis is being able to capture the formation of all the specific low molecular weight products in the C1−C15 size range (products below 215 amu), and this challenge has not been met in the literature thus far.

Therefore, we have developed a polypropylene model that quantifies both the evolution of the polypropylene polymer molecular weight distribution and the formation of specific products in the C1−C15 size range simultaneously. Differential equations tracking the moments of structurally distinct polymer species were developed, and these equations incorporated a wide range of free radical reactions, including reactions leading to specific low molecular weight products. Bond fission, chain-end β-scission, midchain β-scission, intermolecular hydrogen abstraction, radical addition, radical recombination, disproportionation, and intramolecular hydrogen transfer were included. Unique polymer groups were devised that allowed polymeric features to be tracked while maintaining a manageable model size. Polymer species were lumped into various classes, as done previously,[2,21,29−31] to track the presence and location of radical centers, the position of double bonds, and the orientation of the "head" and "tail" ends of the monomer units. The model developed tracked all major low molecular weight products (27 low molecular weight products in the C1−C15 size range were tracked), consisted of over 24 000 reactions, and tracked 213 species. The intrinsic kinetic parameters (a frequency factor and activation energy for each reaction) were obtained from data in the literature and previous modeling work in our laboratory.[1,2] The approach to model construction, the detailed chemistry included, the quantitative parameters used, and comparison to experimental data are discussed below.

Experimental Section

The experimental data collected under isothermal conditions at 350 and 420 °C in our laboratory have been reported previously.[22] The same experimental procedure used to collect that data was employed to gather data at 380 °C. Briefly, batch pyrolysis experiments were carried out by putting polypropylene into a 3.1-mL glass ampule (Wheaton), purging with argon, and flame sealing. Loadings of 20 mg were studied for reaction times from 5 to 180 min. At least two replicates and in most cases three replicates were performed for each reaction time. The polypropylene was obtained from Aldrich (syndiotactic; $M_n = 54\,000$, $M_w = 127\,000$; unstabilized) in powder form. Note that the majority of commercial polypropylene samples are isotactic, but the pyrolysis kinetics of syndiotactic and isotactic polypropylene are similar.[32] While they afford different diastereomers because of the different stereochemistry along the backbone, the amounts of a given alkene or alkane product are the same. Furthermore, as will be shown below, parameters obtained from the literature for pyrolysis of isotactic polypropylene work well for the syndiotactic polypropylene studied here. Conversely, the model we have developed based on the pyrolysis of syndiotactic polypropylene can be used without adjusting any parameters to capture pyrolysis results in the literature for isotactic polypropylene samples.

Products that were gaseous at room temperature from the polypropylene pyrolysis were analyzed by placing the ampule inside a 53-mL flask with a Tygon tube on one end and an injection port on the other. Both ends were then sealed with septa. The flask was purged with helium for 10 min and, after the ampule was broken, the gases were allowed to equilibrate for 30 min. Gas samples were analyzed using gas chromatography.

Liquid and solid products were extracted with 1.5 mL of HPLC grade methylene chloride. The product solution was first filtered and then passed through a gel permeation chromatograph (GPC). Only polypropylene-derived products up to C_{25} were completely soluble in methylene chloride. Products with molecular weights less than 400 g/mol were collected using a fraction collector attached to the GPC outlet. Products were then analyzed by gas chromatography and mass spectrometry. All details of the product analysis are provided in Wong and Broadbelt.[22] Error bars shown in the figures represent the standard deviations of experiments that have been at least duplicated.

Model Development

Mechanistic Chemistry. The method of moments was used to develop differential equations describing

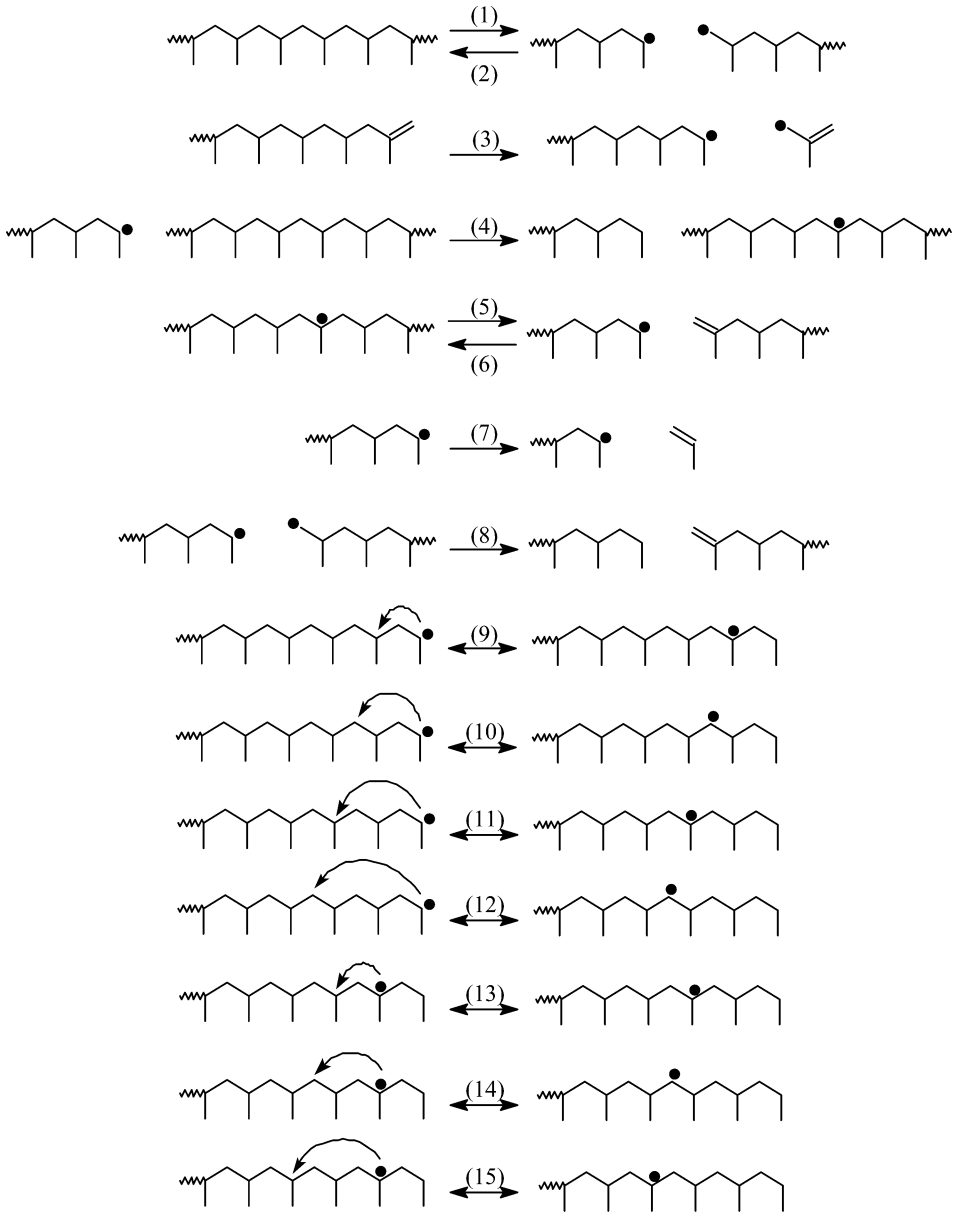

Figure 1. Polypropylene reaction types incorporated into detailed mechanistic model. Reactions types are numbered in the preceding text.

the pyrolysis kinetics, and the mechanistic chemistry of interest was implemented by deriving the terms of the moment equations corresponding to each reaction type.[2,21,30] The terms of the moment equations were derived for the following reactions: (1) chain fission, (2) radical recombination, (3) allyl chain fission, (4) intermolecular hydrogen abstraction, (5) midchain β-scission, (6) radical addition, (7) end-chain β-scission, (8) disproportionation, (9) 1,3-end-hydrogen transfer, (10) 1,4-end-hydrogen transfer, (11) 1,5-end-hydrogen transfer, (12) 1,6-end-hydrogen transfer, (13) 1,3-mid-hydrogen transfer, (14) 1,4-mid-hydrogen transfer, and (15) 1,5-mid-hydrogen transfer. Examples of these reactions for polypropylene are pictured in Figure 1, and the moment equations describing these reactions are given in our previous modeling work.[2]

One key to the formation of low molecular weight products was intramolecular hydrogen transfer reactions. The accessible positions along the polymer backbone were selected based on both theoretical data and experimental data in the literature reporting the relative rates of the various intramolecular hydrogen transfer reactions. In our mechanism, the only backbiting reactions originating from an end-chain radical are the 1,3-, 1,4-, 1,5-, and 1,6-end-hydrogen transfers (reactions 9−12 in Figure 1). Backbiting reactions from end-chain radicals to carbons further down the polymer chain (i.e., seventh carbon position or greater) have been found to be both energetically unfavorable[33,34] and less probable[35] compared to the 1,4-, 1,5-, and 1,6-end-hydrogen transfers. However, it is clear from literature data[25] and data collected in our laboratory[22] that specific radicals at the seventh and ninth carbon positions are being formed due to the significant yields of tetramer and pentamer obtained during polypropylene pyrolysis. For example, data in the literature[25] and data collected in our laboratory[22] show that tetramer and pentamer are among the five products with the highest mass yields.

To account for the formation of radicals at positions further removed from the chain ends, 1,3-, 1,4-, and 1,5-mid-hydrogen transfers (reactions 13−15 in Figure 1) following an end-hydrogen transfer were included. For

Table 1. Labels of Products Tracked in Polypropylene Model

product label	species name
C1	methane
C2	ethane
C3=	propene
C3	propane
C4=	isobutylene
C4	isobutane
C5=	2-pentene
C5	*n*-pentane
C6= (dimer)	2-methyl-1-pentene 4-methyl-2-pentene
C6	2-methyl-1-pentane
C7= =	2,4-dimethyl-1,4-pentadiene
C7=	2,4-dimethyl-1-pentene
C7	2,4-dimethylpentane
C8=	4-methyl-2-heptene
C8	4-methylheptane
C9= (trimer)	2,4-dimethyl-1-heptene 4,6-dimethyl-2-heptene
C9	2,4-dimethylheptane
C10= =	2,4,6-trimethyl-1,6-heptadiene
C10=	2,4,6-trimethyl-1-heptene
C10	2,4,6-trimethylheptane
C11=	4,6-dimethyl-2-nonene
C11	4,6-dimethylnonane
C12= (tetramer)	2,4,6-trimethyl-1-nonene 4,6,8-trimethyl-2-nonene
C13= =	2,4,6,8-tetramethyl-1,8-nonadiene
C13=	2,4,6,8-tetramethyl-1-nonene
C14=	4,6,8-trimethyl-2-undecene
C15= (pentamer)	2,4,6,8-tetramethyl-1-undecene 4,6,8,10-tetramethyl-2-undecene

mid-hydrogen transfer reactions, the midchain radicals produced from the initial 1,3-, 1,4-, and 1,5-end-hydrogen transfers undergo an additional hydrogen transfer step, thereby forming specific radicals on the seventh through the ninth carbons. These 1,3-, 1,4-, and 1,5-mid-hydrogen transfers are slower than the original 1,3-, 1,4-, and 1,5-end-hydrogen transfers due to entropic factors, but they are significant enough to produce midchain radicals further down the chain. Specific midchain radicals near the end of a polymer chain are also produced by the random intermolecular abstraction of hydrogen (reaction 4 in Figure 1), and these reactions are included within the model. However, the amount of specific midchain radicals produced through intermolecular hydrogen abstraction is very small compared to intramolecular hydrogen abstraction due to the large number of hydrogens available for abstraction along the backbone of the high molecular weight polymer chains. Overall, the mechanism we have proposed only uses conventional 1,3-, 1,4-, 1,5-, and 1,6-hydrogen transfers.

By use of these free radical reaction types and keeping track of specific radicals, the evolution of 27 low molecular weight products in the C1−C15 size range (products below 215 amu) was followed in the model. These products are listed in Table 1. Note that the dimer (C6=), trimer (C9=), tetramer (C12=), and pentamer (C15=) labels in Table 1 each represent two isomers that are lumped together in the model results to obtain the yields of these species. The experimental data for all species larger than C5 (including dimer, trimer, tetramer, and pentamer) represent the sum of the yields of all the isomers for these species if multiple isomers were detected. Figures 2, 3, and 4 show all the specific midchain radicals formed by either 1,3-, 1,4-, 1,5-, and 1,6-end-hydrogen transfers or 1,3-, 1,4-, and 1,5-mid-hydrogen transfers and the products that are formed. Figure 2 shows the products formed from radicals on odd carbon numbers near the end of chain, which are the major products formed during polypropylene pyrolysis. Figure 3 shows the products formed from radicals on even carbon numbers, which are all the minor products tracked. Figure 4 shows specific radicals near unsaturated chain ends that were required to track the formation of isobutylene, 2-pentene, and low molecular weight dienes.

Branching reactions were also included in the model, where end-chain radicals were allowed to recombine with midchain radicals. The approach outlined by McCoy and Wang for describing random and proportioned chain fission and β-scission reactions[11,17] was implemented into the moment equations. Chain fission and midchain β-scission of polymer chains were assumed to be random processes.

Specification of Rate Constants. Incorporation of these free radical elementary step reactions in a model of polymer pyrolysis required the specification of the rate parameters. The same approach used previously in our work to quantify rate constants was adopted.[36] The rate parameters were dependent on not only the reaction type but also the structural characteristics of the reactants and products. Assuming the validity of the Arrhenius relationship, a frequency factor and an activation energy for each reaction were specified. Each reaction of a given type (e.g., bond fission) shared the same frequency factor. The activation energy for each specific reaction was calculated using the Evans−Polanyi relationship,[37] in which the activation energy is related linearly to the heat of reaction, i.e., $E = E_o + \alpha\Delta H_R$. The values of the heats of reaction were obtained from experimental polymerization data or based on analogous reactions of molecular mimics of the polymer structure as used previously.[36,38,39]

A summary of the frequency factors, Evans−Polanyi constants, and heats of reaction for the main pyrolysis reactions for polypropylene is provided in Table 2. Note that no optimization of the frequency factors or activation energies was carried out. The majority of the frequency factors and the parameters E_o and α for each reaction type were taken directly from our previous work.[1,2] The frequency factor for β-scission was obtained using thermodynamic data in the literature.[40] In addition, the frequency factors for 1,3-end-hydrogen transfer and 1,5-end-hydrogen transfer were obtained by matching the model results to the ratios reported in the literature of trimer to monomer (5.5:1) and dimer to monomer (1.4:1) for the pyrolysis of polypropylene at 388 °C.[41] The intrinsic barriers for the 1,4- and 1,6-end-hydrogen transfers were then estimated by adding the strain energy for five-membered and seven-membered rings,[34] respectively, to the intrinsic barrier for the 1,5-end-hydrogen transfer reaction. The frequency factors for 1,3-, 1,4-, and 1,5-mid-hydrogen transfers were obtained by matching the model results to the ratio of tetramer to monomer (1.5:1) for the pyrolysis of polypropylene at 388 °C reported in the literature.[41] It was assumed that all ratios of the midchain hydrogen transfer frequency factors to their corresponding end-chain hydrogen transfer frequency factors were equal.

The diffusion dependence of termination reactions was implemented using Smoluchowski's equation[42] for the rate constant of a diffusion-controlled reaction. The termination rate constant was assumed to be inversely proportional to the chain length of the terminating radicals, and a termination rate constant was calculated

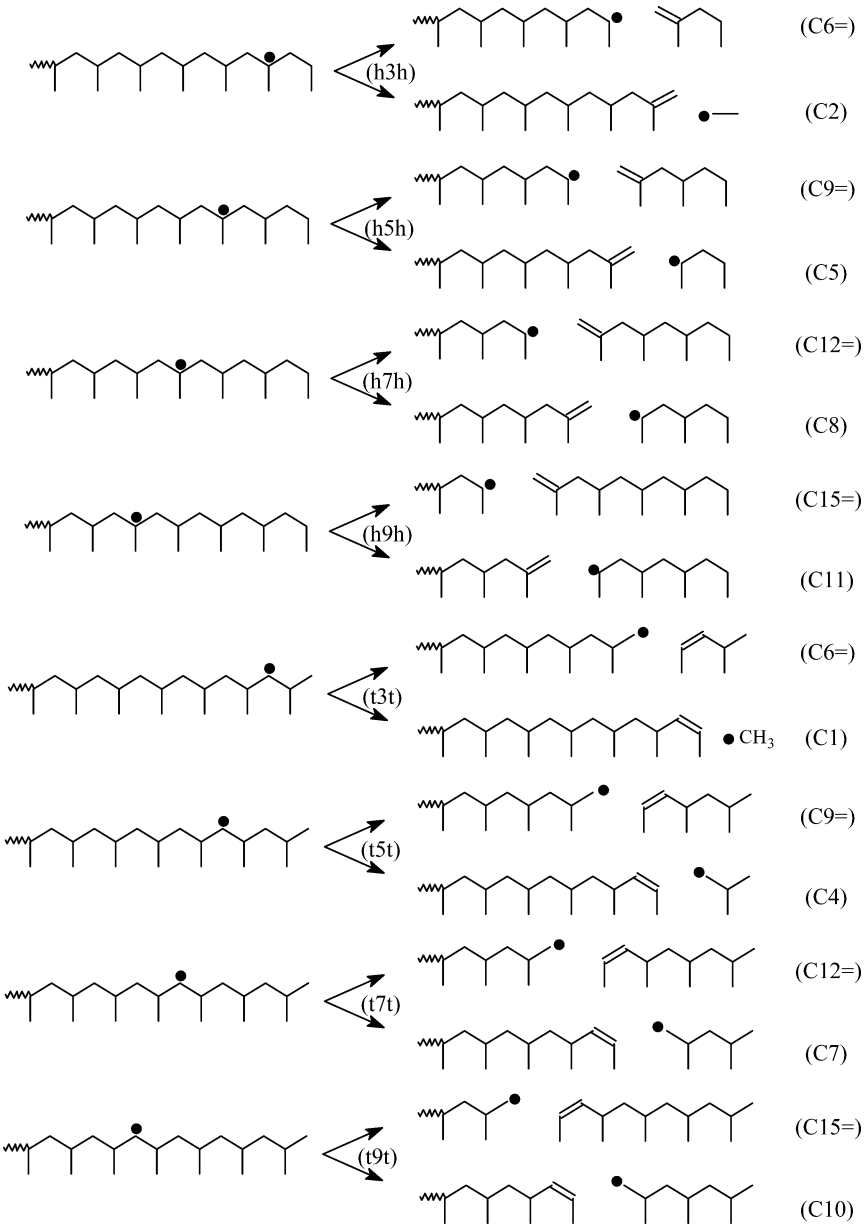

Figure 2. Midchain β-scission reactions of specific midchain radicals located three, five, seven, and nine carbons from the end of a chain. The β-scission of these specific midchain radicals leads to the formation of unsaturated oligomers and saturated low molecular weight radicals (labeled to the right of the products). The labels on the arrows represent the type of midchain radical undergoing β-scission, where the first letter represents the type of midchain radical ((t) tail or (h) head saturated), the number represents the distance in number of carbon atoms from the end of the chain, and the final letter represents the type of end group ((t) tail or (h) head saturated).

for all termination reactions using the average length of all the polymer radicals present in the polymer melt. In addition, hydrogen abstraction rate constants were assumed to be inversely proportional to the size of the abstracting radical.[43]

Model Assembly and Solution. To choose what polymer species to track, a lumping scheme was devised that lumped polymer species into groups based on their end-chain structure. The different types of end-chain groups possible for polypropylene are shown in Figure 5, and all of these features were tracked within the model. In addition, four different types of radicals were tracked within the model. Both head and tail end-chain radicals were distinguished within the model since both of these radical types are formed during bond fission (reaction 1 in Figure 1). In addition, both head and tail midchain radicals were tracked since both of these radical types are formed during hydrogen abstraction and intramolecular hydrogen transfer reactions. Examples of head and tail midchain radicals are shown in Figures 2−4. However, the methyl substituent groups were assumed to be inert and not participate in the free radical chemistry since the abstraction of hydrogen from the methyl substituent groups would result in the formation of unstable primary radicals. Instead, it is more energetically favorable that tertiary or secondary hydrogen atoms are abstracted during intermolecular hydrogen abstraction and intramolecular hydrogen transfer reactions, which produce head and tail midchain radicals, respectively. The bond strength of the primary hydrogen atoms on the methyl substituent groups is 5.9 kcal/mol stronger than the tertiary hydrogen atoms and 2.8 kcal/mol stronger than the secondary hydrogen atoms on the backbone of the polypropylene chains.

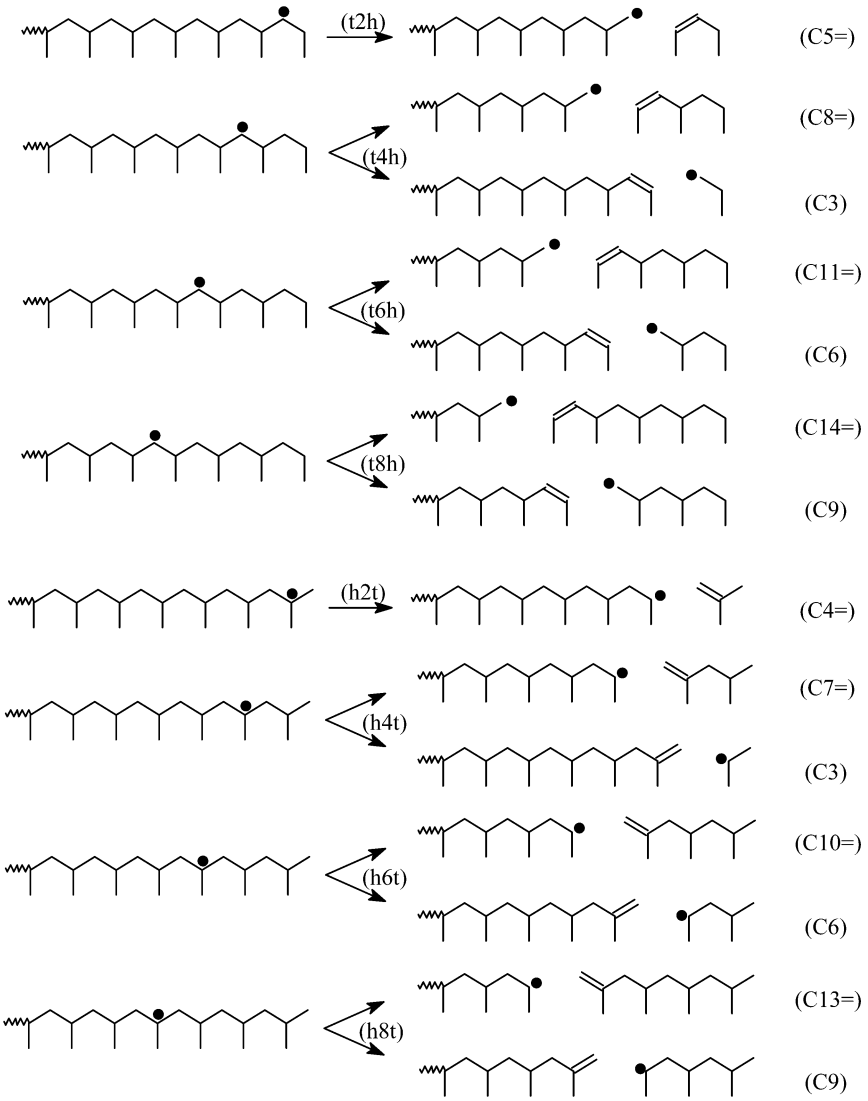

Figure 3. Midchain β-scission reactions of specific midchain radicals located two, four, six, and eight carbons from the end of a chain. The β-scission of these specific midchain radicals leads to the formation of unsaturated oligomers and saturated low molecular weight radicals (labeled to the right of the products). The labels on the arrows represent the type of midchain radical undergoing β-scission, where the first letter represents the type of midchain radical ((t) tail or (h) head saturated), the number represents the distance in number of carbon atoms from the end of the chain, and the final letter represents the type of end group ((t) tail or (h) head saturated).

To include branching, all branched species were lumped into linear polymer groups since the amount of branching that occurs during polypropylene pyrolysis is extremely minor. Forming branches by radical addition onto midchain radicals is negligible due to the fast rate of the reverse β-scission reaction. Thus, branches are primarily formed from the recombination of an end-chain radical and a midchain radical, which leads to a very small amount of branching but is a very significant reaction pathway since it terminates radicals. Upon recombination of end-chain and midchain radicals, the species formed were lumped into the dead polymer group with the same end-chain groups as the original midchain radical.

The model also tracked structural irregularities within polymer chains. All atypical bonds (tail−tail and head−head) were tracked explicitly, and using the concentrations of the different types of bonds, probabilities were incorporated into the model to partition fission reactions between possible breaking bonds. In addition, different heats of reaction were used to characterize each possible bond fission reaction.

To aid in model construction, a program written in the Perl programming language was developed to construct a list of the chemical reactions from minimal user input. Another Perl program was then developed which could transform this list into moment rate terms. These terms were then assembled into a set of ordinary differential equations that included three (zeroth, first, and second) moment equations for each unique species. The resultant set of stiff differential equations was then solved using DASSL.[44]

Polypropylene Pyrolysis Modeling. Prediction of Low Molecular Weight Products. The 27 low molecular weight products tracked within the model represent all of the products in the C1−C15 size range (products below 215 amu) observed experimentally during polypropylene pyrolysis to moderate conversion (except for small amounts of C14 alkane and aromatics). Because polypropylene products below 215 amu are volatile at the reaction conditions employed in our batch pyrolysis experiments (<5 bar and 350−420 °C), they were assumed to evaporate immediately upon being formed and not interact further with the degrading

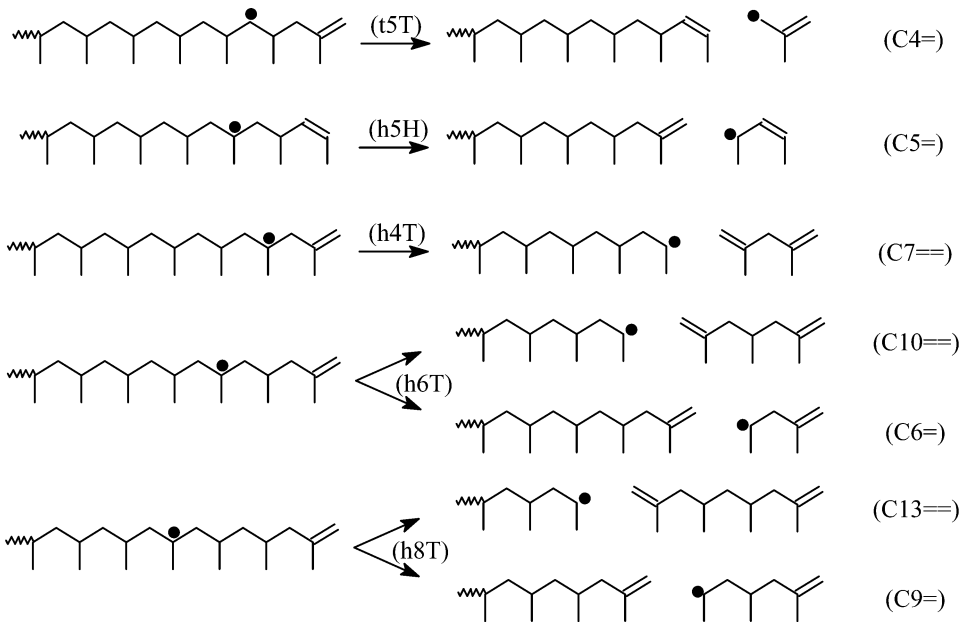

Figure 4. Midchain β-scission reactions of specific midchain radicals near unsaturated chain ends. The β-scission reactions of the t5T and h5H radicals produce stable allylic radicals, while the β-scission reactions of the other radicals above produce dienes and dimeric and trimeric radicals (labeled to the right of the products). The labels on the arrows represent the type of midchain radical undergoing β-scission, where the first letter represents the type of midchain radical ((t) tail or (h) head saturated), the number represents the distance in number of carbon atoms from the end of the chain, and the final letter represents the type of end group ((t) tail or (h) head unsaturated).

Table 2. Representative Values of Kinetic and Thermodynamic Parameters for Reaction Types Incorporated into Mechanistic Model of Polypropylene Pyrolysis[a]

reaction type	frequency factor, A (s^{-1} or L mol^{-1} s^{-1})	intrinsic barrier, E_o (kcal mol^{-1})	transfer coefficient	representative heat of reaction (kcal mol^{-1})	activation energy (kcal mol^{-1})
chain fission	1.0×10^{16}	2.3	1.0	79.7	82.0
chain fission allyl	5.5×10^{13}	2.3	1.0	68.7	71.0
radical recombination	1.1×10^{11}	2.3	0.0	−79.7	2.3
disproportionation	1.1×10^{10} [g]	2.3	0.0	NA	2.3
end-chain β-scission	9.4×10^{14} [b]	11.4	0.76	21.9[b]	28.0
midchain β-scission	9.4×10^{14} [b]	11.4	0.76	22.0	28.1
radical addition	1.5×10^{7}	11.4	0.24	−22.0	6.1
hydrogen abstraction	1.0×10^{8}	12.0	0.30−0.70[f]	−3.1	10.5
1,3-end-hydrogen transfer	2.0×10^{14} [c]	25.0	0.30−0.70[f]	−2.8 or −3.1	23.6 or 23.5
1,4- end-hydrogen transfer	2.0×10^{11}	18.5[d]	0.30−0.70[f]	0.0 or −5.9	18.5 or 15.6
1,5- end-hydrogen transfer	1.0×10^{11} [c]	12.0	0.30−0.70[f]	−2.8 or −3.1	10.6 or 10.5
1,6- end-hydrogen transfer	2.0×10^{10}	18.3[d]	0.30−0.70[f]	0.0 or −5.9	18.3 or 15.4
1,3-mid-hydrogen transfer	5.0×10^{12} [e]	25.0	0.30−0.70[f]	0.0	25.0
1,4-mid-hydrogen transfer	5.0×10^{9} [e]	18.5[d]	0.30−0.70[f]	3.1 or −3.1	20.1 or 17.0
1,5-mid-hydrogen transfer	2.5×10^{9} [e]	12.0	0.30−0.70[f]	0.0	12.0

[a] All rate parameters without footnotes were obtained from previous modeling work in our laboratory,[1,2] and all heats of reaction without footnotes were obtained from the NIST database.[39] [b] Calculated from ΔS_r and ΔH_r for polymerization from ref 40. [c] Estimated to fit ratios of trimer and dimer to monomer yield from data obtained by Chien and Kiang, 1978.[41] [d] Obtained from strain energy of 1,4- and 1,6-end-hydrogen transfers relative to 1,5-end-hydrogen transfer.[34] [e] Estimated to fit ratio of tetramer to monomer yield from data obtained by Chien and Kiang, 1978.[41] [f] Calculated using the Blowers and Masel equation.[46] [g] Disproportionation estimated to be 10% of recombination rate.[47]

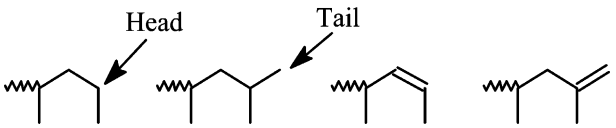

Figure 5. End-chain types are distinguished based on their head/tail and unsaturated/saturated end-chain structure.

polymer melt. Low molecular weight radicals, however, were assumed to react within the polymer melt before evaporating. Semibatch reactor equations were employed to track the volume shrinkage of the polymer melt as low molecular weight products were evolved. Further transformations among species partitioned into the gas phase were not incorporated into the model since the ratio of the gas-phase volume to the melt-phase volume was high and the sample loadings were extremely low. This assumption was invalid only at the highest reaction temperature where high conversions were achieved. As noted below, significant secondary reactions are anticipated only at 420 °C above 50% conversion.

The model results in comparison to experimental data for the pyrolysis of polypropylene at 350 °C are shown in Figure 6 and Table 3. In Figure 6, the experimental yields of the five major alkenes, five major alkanes, and total low molecular weight products (LMWPs) in the C1−C15 size range are compared to model yields as a function of time. The model results are in reasonably good agreement with the experimental yields for these major products; the majority of the model results are

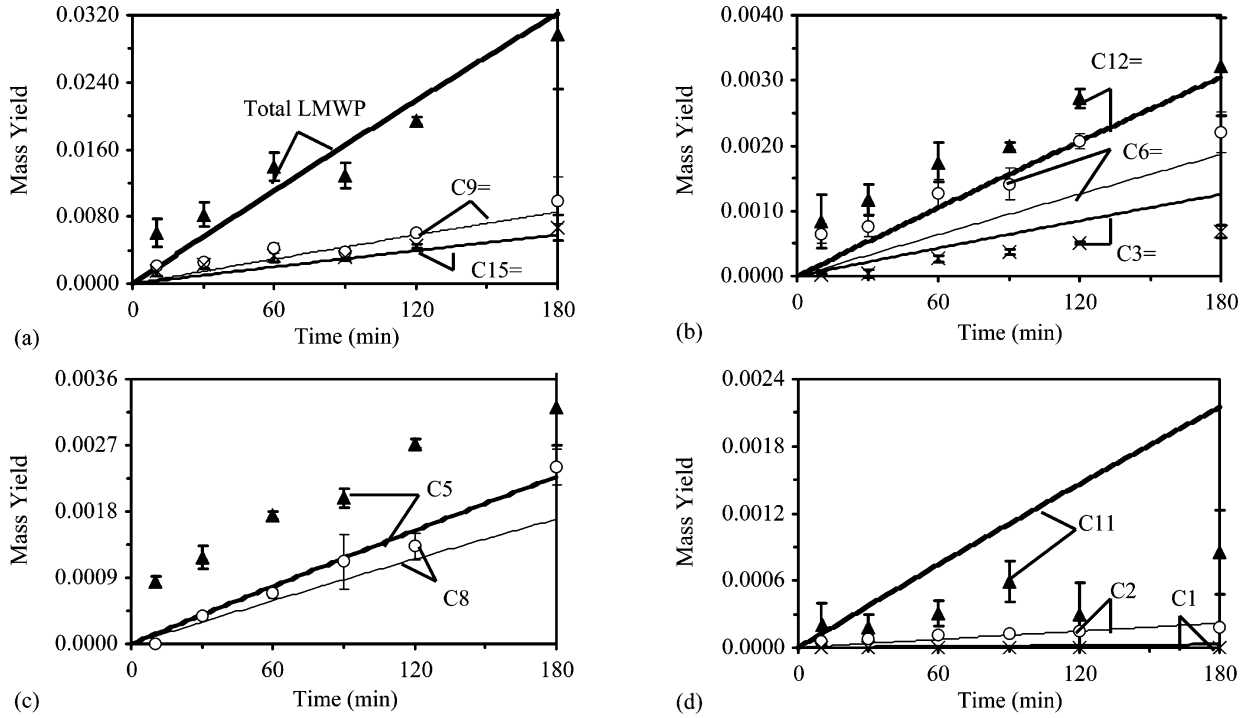

Figure 6. Comparison of model results to experimental data for the pyrolysis of polypropylene at 350 °C for the mass yields of (a) C9═, C15═, and total LMWP (all C1−C15); (b) C3═, C6═, and C12═; (c) C5 and C8; and (d) C1, C2, and C11.

Table 3. Comparison of Model Results to Experimental Data for the Mass Yields of the 27 Main Low Molecular Weight Products Formed during Polypropylene Pyrolysis at 350 °C

	% mass yield			
	120 min		180 min	
product tracked	exptl	model	exptl	model
C1	0.000	0.002	0.000	0.003
C2	0.015	0.015	0.018	0.022
C3═	0.051	0.085	0.068	0.125
C3	0.000	0.018	0.000	0.026
C4═	0.000	0.004	0.015	0.007
C4	0.000	0.028	0.000	0.040
C5═	0.000	0.003	0.000	0.004
C5	0.272	0.154	0.322	0.227
C6═	0.206	0.126	0.221	0.186
C6	0.000	0.011	0.000	0.016
C7══	0.000	0.001	0.000	0.002
C7═	0.000	0.054	0.000	0.079
C7	0.000	0.039	0.000	0.057
C8═	0.000	0.020	0.000	0.030
C8	0.133	0.115	0.241	0.170
C9═	0.613	0.579	0.992	0.855
C9	0.000	0.034	0.000	0.049
C10══	0.000	0.001	0.000	0.002
C10═	0.000	0.019	0.000	0.028
C10	0.000	0.056	0.000	0.082
C11═	0.000	0.010	0.000	0.015
C11	0.029	0.146	0.085	0.215
C12═	0.171	0.206	0.300	0.305
C13══	0.000	0.001	0.023	0.002
C13═	0.000	0.040	0.000	0.058
C14═	0.000	0.020	0.000	0.030
C15═	0.448	0.395	0.666	0.582
C1−C15 total yield	1.937	2.182	2.968	3.220

within a factor of 1.25 of the experimental yields, and all the model results are within a factor of 2 of the experimental data. Much of the scatter in the experimental data in Figure 6 is due to the difficulty in obtaining experimental data at such low conversions. In addition, it is possible that structural irregularities in the initial polymer that have not been taken into account in the model results shown in Figure 6 are impacting the pyrolysis behavior. As will be shown below, a very small fraction of weak links in the initial polymer structure can change the initial slope of the evolution of the product yields, but the slope after a rapid initial rise is similar regardless whether the model does or does not include weak links. This effect is clearly manifested in the C5 yield in Figure 6, where the model results do not rise as quickly initially as the experimental data, but the model has the same slope as the data over long times. In addition, it will be shown below that 350 °C is the highest temperature where the effect of weak links would be observed.

In Table 3, the specific mass yields for all 27 low molecular weight components tracked in the model are compared to the experimental yields obtained for these products at 350 °C after 120 and 180 min of pyrolysis. Due to the low conversion observed at 350 °C, the yields of most of the products are lower than the minimum mass yield that can be quantified with the given experimental protocol (i.e., 0.00005), and thus most of the experimental mass yields are zero even after 180 min of pyrolysis. However, for the products that were detected and quantified, the model yields are in very good agreement with the experiments.

The model results in comparison to experimental data for the pyrolysis of polypropylene at 380 °C are shown in Figure 7 and Table 4. In Figure 7, the experimental yields of the five major alkenes, five major alkanes, and total LMWPs in the C1−C15 size range are compared to model yields as a function of time. The model results are in good agreement with the experimental data, where all of the predicted yields of the major products in Figure 7 are within a factor of 1.7 of the experimental yields, and most are within a factor of 1.25. Because of the higher mass yields, there is considerably less scatter in the experimental data than that observed in Figure 6.

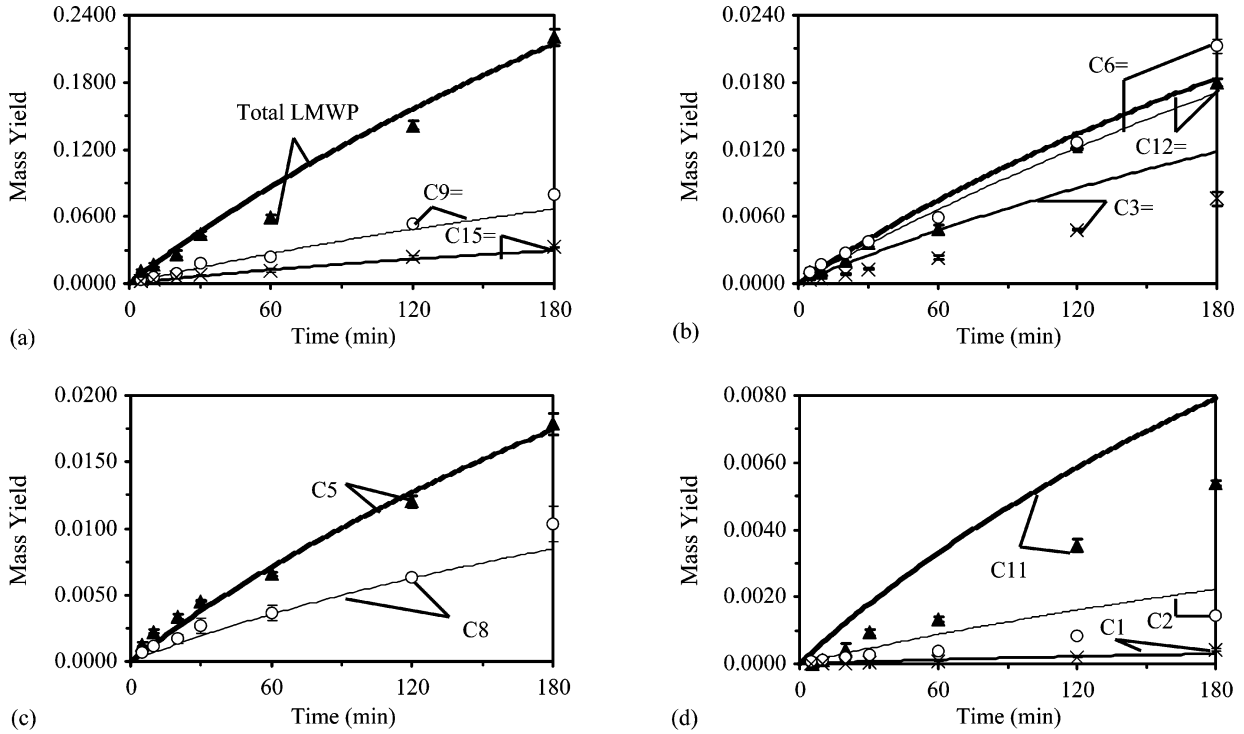

Figure 7. Comparison of model results to experimental data for the pyrolysis of polypropylene at 380 °C for the mass yields of (a) C9═, C15═, and Total LMWP (all C1−C15); (b) C3═, C6═, and C12═; (c) C5 and C8; and (d) C1, C2, and C11.

Table 4. Comparison of Model Results to Experimental Data for the Mass Yields of the 27 Main Low Molecular Weight Products Formed during Polypropylene Pyrolysis at 380 °C

	% mass yield			
	120 min		180 min	
product tracked	exptl	model	exptl	model
C1	0.020	0.022	0.042	0.030
C2	0.083	0.160	0.144	0.222
C3═	0.483	0.854	0.757	1.177
C3	0.029	0.141	0.063	0.192
C4═	0.186	0.045	0.354	0.073
C4	0.000	0.263	0.000	0.352
C5═	0.036	0.036	0.072	0.060
C5	1.202	1.271	1.788	1.743
C6═	1.262	1.217	2.122	1.706
C6	0.006	0.069	0.050	0.092
C7══	0.035	0.049	0.180	0.094
C7═	0.078	0.400	0.196	0.547
C7	0.000	0.271	0.000	0.358
C8═	0.146	0.166	0.390	0.234
C8	0.633	0.625	1.037	0.846
C9═	5.357	4.835	7.973	6.658
C9	0.147	0.150	0.195	0.201
C10══	0.005	0.048	0.042	0.094
C10═	0.063	0.126	0.129	0.171
C10	0.000	0.309	0.000	0.406
C11═	0.075	0.071	0.137	0.099
C11	0.351	0.585	0.538	0.791
C12═	1.266	1.337	1.796	1.836
C13══	0.107	0.047	0.243	0.092
C13═	0.066	0.195	0.100	0.262
C14═	0.059	0.118	0.073	0.162
C15═	2.397	2.189	3.262	2.957
C1−C15 total yield	14.149	15.599	22.029	21.455

In Table 4, the specific mass yields for all 27 components tracked in the model are compared to the experimental yields obtained for these products at 380 °C after 120 and 180 min of pyrolysis. At 380 °C, most of the products listed in Table 4 were detected and quantified experimentally with the exception of C4, C7, and C10. While the model results for the major products (the 10 products analyzed in Figure 7) are in good agreement with the experimental data, the model results for the minor products (the 17 products not analyzed in Figure 7) are mixed. Of these 17 minor products tracked, the model yields are within a factor of 2 of the experimental yields for 7 of the minor products and a factor of 3 for 13 of the minor products. However, there are some trends within the minor product yields that are unexpected and contradict the model results. For example, C4, C7, and C10 were not detected during our pyrolysis experiments, while C1 was detected. On the basis of our mechanism in Figure 2, these four species are all formed from analogous reactions, where midchain β-scission occurs after the formation of a secondary midchain radical near the tail end of a polypropylene chain (β-scission of midchain radicals t3t, t5t, t7t, and t9t in Figure 2). Therefore, the presence of C1 and the absence of C4, C7, and C10 in the final experimental product distribution appear to be inconsistent. While there are some discrepancies between the model and experimental results, the model does track 27 low molecular weight products and predicts the most significant products and their temporal behavior reasonably well. Some of the discrepancies between the experimental data and the model predictions for the 17 minor products are likely due to the error involved when determining the quantitative yields of species in low concentration.

The model results for the pyrolysis of polypropylene at 420 °C are compared to experimental data in Figure 8 and Table 5. In Figure 8, the experimental yields of the five major alkenes, five major alkanes, and total LMWPs in the C1−C15 size range are compared to the model yields as a function of time. The model results are in good agreement with the experimental yields for all of the data shown in Figure 8, where the predicted yields are within a factor of 1.7 of the experimental yields for all of the major products, and most are within

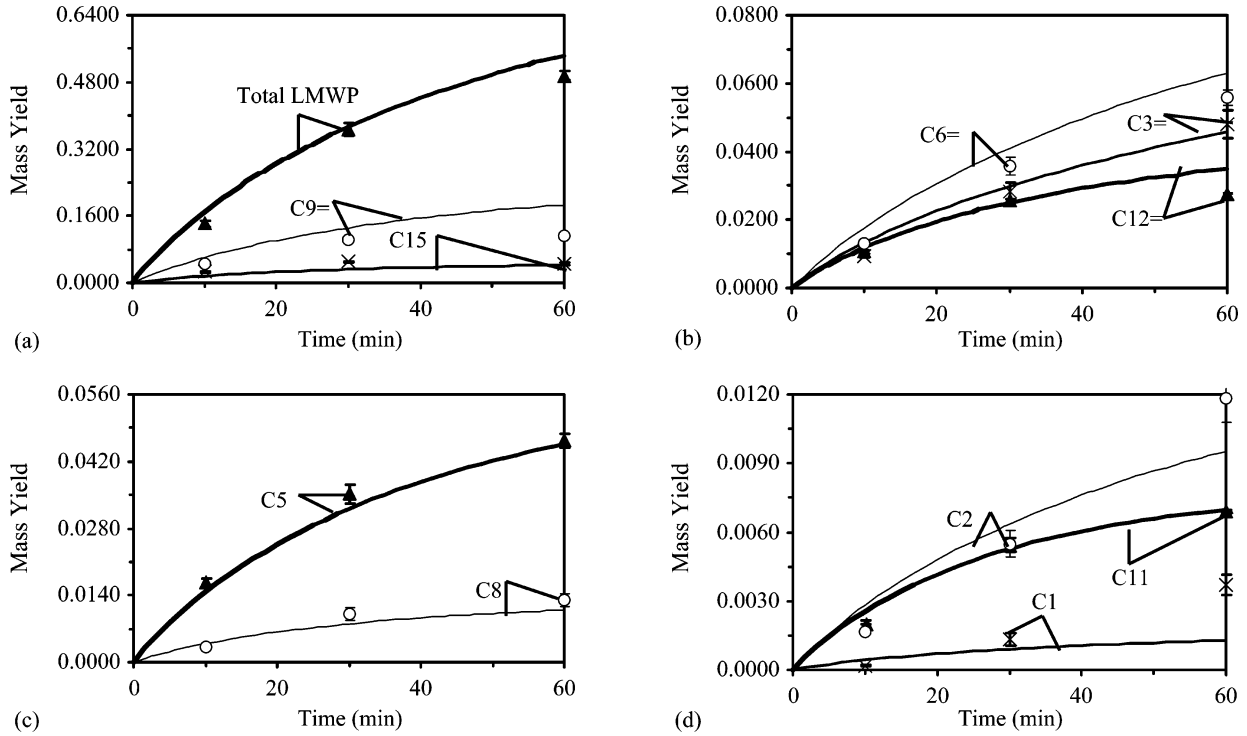

Figure 8. Comparison of model results to experimental data for the pyrolysis of polypropylene at 420 °C for the mass yields of (a) C9═, C15═, and Total LMWP (all C1−C15); (b) C3═, C6═, and C12═; (c) C5 and C8; and (d) C1, C2, and C11.

Table 5. Comparison of Model Results to Experimental Data for the Mass Yields of the 27 Main Low Molecular Weight Products Formed during Polypropylene Pyrolysis at 420 °C

	% mass yield			
	30 min		60 min	
product tracked	exptl	model	exptl	model
C1	0.131	0.091	0.371	0.129
C2	0.550	0.634	1.182	0.954
C3═	2.843	2.988	4.792	4.565
C3	0.199	0.378	0.547	0.548
C4═	1.246	0.180	2.674	0.382
C4	0.000	0.840	0.000	1.135
C5═	0.320	0.168	0.797	0.377
C5	3.526	3.205	4.638	4.557
C6═	3.575	4.101	5.570	6.302
C6	0.100	0.118	0.272	0.163
C7══	0.451	0.302	0.469	0.721
C7═	0.532	0.986	0.951	1.434
C7	0.000	0.507	0.145	0.654
C8═	0.771	0.466	1.167	0.750
C8	1.012	0.807	1.296	1.086
C9═	10.236	13.174	11.228	18.639
C9	0.411	0.166	0.446	0.227
C10══	0.117	0.314	0.138	0.797
C10═	0.263	0.265	0.354	0.378
C10	0.000	0.413	0.000	0.523
C11═	0.396	0.160	0.811	0.239
C11	0.544	0.528	0.693	0.698
C12═	2.558	2.504	2.763	3.485
C13══	0.619	0.295	0.603	0.728
C13═	0.244	0.261	0.339	0.357
C14═	0.172	0.189	0.371	0.263
C15═	5.051	3.258	4.541	4.270
C1−C15 total yield	36.724	37.297	49.485	54.359

a factor of 1.25. After 60 min of pyrolysis, gas-phase reactions become significant due to the large concentration of oligomers in the gas phase within the closed batch reactor system. This results in the decrease in yields of large oligomers such as trimer, tetramer, and pentamer after 60 min of pyrolysis and the formation of aromatic species. Due to these gas-phase reactions, the trimer experimental yield begins to level off after 60 min of pyrolysis as shown in Figure 8.

In Table 5, the specific mass yields for all 27 components tracked in the model are compared to the experimental yields obtained for these products at 420 °C after 30 and 60 min of pyrolysis. At 420 °C, all of the products listed in Table 5 were detected and quantified experimentally except for C4 and C10. Similar to the results in Table 4, the model results for the major products (the 10 products analyzed in Figure 8) are in good agreement with the experimental data, while the model results for the minor products (the 17 products not analyzed in Figure 8) are in reasonable agreement. Of the 17 minor products tracked, the model yields are within a factor of 2 of the experimental data for 11 of the products. However, like the model results at 380 °C, the model was unable to capture the experimental yields of C4, C4═, C7, and C10. Overall, the results once again show the ability of the model to capture the general features of the experimental product distribution. In addition, if the model is run to complete conversion at 420 °C, the product distribution of species in the C1−C15 size range is comprised of 74.1 wt % alkenes, 17.5 wt % alkanes, and 8.4 wt % dienes. This final product distribution is similar to the composition of the final product distributions obtained in the literature[25,27] in reactor configurations that were not complicated by secondary reactions.

A closer look at the experimental data in Tables 3−5 reveals some interesting trends. First, at all three temperatures it is evident that of the nine products that are observed experimentally with the highest yields, only propene (C3═) is not formed due to β-scission of a radical on the third, fifth, seventh, or ninth carbon position from the end of a chain. This indicates that specific midchain radicals on the odd carbon positions are favored over the even carbon positions during

polypropylene pyrolysis. Second, the experimental data show that pentamer usually has the second highest mass yield after trimer. This result would not be expected based on mechanisms put forth in the literature, where it has been postulated that pentamer is formed after the formation of a specific radical at the ninth carbon position directly from an end-chain radical via a 1,9-end-hydrogen transfer. However, this has been found to be extremely unfavorable relative to other end-chain intramolecular hydrogen transfers.[35]

In contrast to literature suggestions, the mechanism implemented into our polypropylene model was able to capture both the high yields of pentamer and the preference for odd-numbered carbon atoms proximate to chain ends. Pentamer is formed via successive 1,5-hydrogen transfer reactions. A 1,5-end-hydrogen transfer reaction is followed by a 1,5-mid-hydrogen transfer to produce a midchain radical at the ninth carbon position. 1,5-Intramolecular hydrogen transfer is the most favorable of all possible 1,*x*-hydrogen transfer reactions, where *x* is 3, 4, 5, or 6. Note that excellent agreement between the model and experimental yields of pentamer was obtained without fitting any experimental data in the literature for the yield of pentamer. Preferences among the various intramolecular hydrogen transfer reactions are also the origin of the preference for the odd-numbered carbon positions near chain ends. The rates of hydrogen transfer to the third and fifth carbon positions are faster than the rates to the fourth and sixth carbon positions (based on the rate parameters in Table 2). From the third and fifth carbon positions, the seventh and ninth carbon positions can be reached by 1,3- and 1,5-mid-hydrogen transfers to lead to the production of tetramer and pentamer. Subsequent 1,3-, 1,4-, and 1,5-mid-hydrogen transfers from carbons in the sixth through ninth positions to carbons even further down the chain are likely slow due to the increase in steric hindrance as the tail attached to the radical lengthens. This agrees with experimental data in our laboratory which shows that the formation of hexamer and larger oligomers is minor compared to the low molecular weight oligomers in the C1−C15 size range.[22]

Prediction of Polymer Molecular Weights. In a study by Chan and Balke,[3] the evolution of the molecular weight distribution was determined for the pyrolysis of polypropylene (M_n = 59 300 g/mol, M_w = 234 000 g/mol) at 275, 300, 315, and 325 °C. Using a simple kinetic model, they determined an overall activation energy that was one-half (~30 kcal/mol compared to ~60 kcal/mol) the typical activation energy for polypropylene pyrolysis reported by other researchers, and they proposed that their lower activation energy was due to the presence of weak links in the polypropylene samples they degraded. However, they were unable to detect weak links in their polypropylene samples using FTIR.

To determine what effect weak links would have on polypropylene pyrolysis, we have modeled the molecular weight data collected by Chan and Balke both with and without weak links incorporated into our polypropylene model. Chan and Balke proposed that the weak links were peroxide linkages (−O−O−) along the backbone of polypropylene chains. These peroxide bonds likely originate from oxygen contamination during the polymerization process, where a small amount of oxygen undergoes propagation to form the peroxide bond.

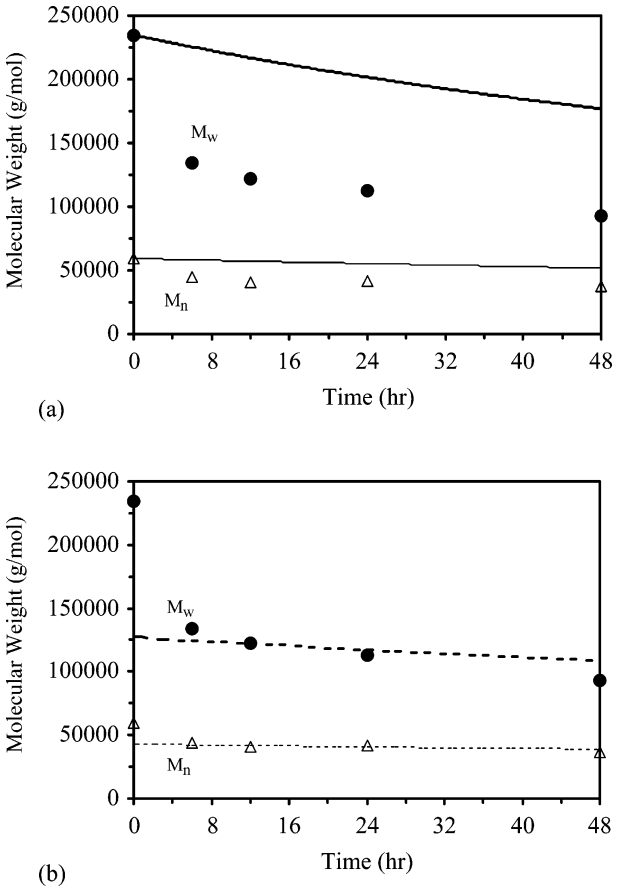

Figure 9. Comparison of model results to experimental molecular weight data in the literature[3] for the pyrolysis of polypropylene (M_n = 59 300 g/mol; M_w = 234 000 g/mol) at 275 °C for (a) no weak links included in the model and (b) peroxide weak links included. In (a) the solid lines represent the model results without weak links and in (b) the dotted lines represent the model results with weak links included. The model results with weak links included overlap the *y*-axis during the beginning of the pyrolysis.

To incorporate these weak links into the model, it was assumed that the initial polymer had a small amount of peroxide bonds within a fraction of the chains. These bonds were assigned a bond strength of 37.0 kcal/mol based on the strength of peroxide bonds in small hydrocarbon molecules.[45] This heat of reaction for O−O bond fission was then used to determine the rate constant for cleavage of these bonds using the Evans−Polyani parameters in Table 2 for chain fission. Since our polypropylene model tracks different types of bonds (i.e., head−tail, tail−tail, and head−head), the peroxide bond was simply added to the model as an additional bond type to track the consumption of peroxide linkages. However, the breakage of a peroxide bond was assumed to form two carbon-centered tail radicals in order to avoid having to track hydroxy ends within the model. Adding a fifth end-chain type would have more than doubled the size of the model. In addition, end-chain oxygen radicals and end-chain primary carbon radicals have similar hydrogen abstraction rates, which is the main reaction the oxygen radicals undergo after breakage of the peroxide bond.

A comparison of the model results to data collected by Chan and Balke at 275 °C is shown in Figure 9. Results of the model both with and without weak links are shown. As is evident from Figure 9a, the model without weak links is unable to capture the initial sharp

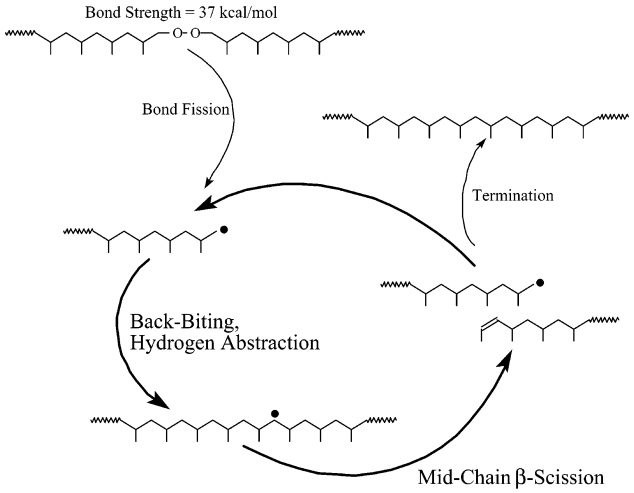

Figure 10. Reaction pathways for radicals produced from the breakage of peroxide bonds within polypropylene chains. The thickness of the arrows indicates the relative rates of reaction, where the slowest steps are the bond fission and termination reactions.

drop in the molecular weight data. However, the slope of the molecular weight results from the model is very similar to the slope of the experimental data. A small concentration of weak links was then added to the model until the model results matched the experimental molecular weight data. To match the experimental data, the initial concentration of weak links in the model was set to approximately one peroxide bond for every 500 000 tail−head bonds. This amount can also be expressed as one chain in every 180 chains having one peroxide bond initially. This small amount of peroxide bonds is likely difficult to detect experimentally, and Chan and Balke believed that the concentration of weak links present in their polypropylene samples was below the detection limit of the FTIR methods they employed. As is evident from Figure 9b, the model with weak links was able to capture the initial sharp drop in the data very well for both the M_n and M_w experimental data. Note that this agreement between the model results and the experimental data did not require any adjustment of the kinetic parameters.

The model results at 275 °C indicate that all of the weak peroxide bonds undergo bond fission during the first few minutes of pyrolysis. However, even though the concentration of peroxide bonds is very small (1 bond per 180 chains), the fission of these peroxide bonds results in the subsequent breakage of 38% of the polymer chains through midchain β-scission reactions. Within the model results, the polypropylene number average molecular weight drops from 59 300 to 43 000 g/mol in the first few minutes. This large drop in M_n is solely due to the presence of a very small amount of weak links via the chemistry illustrated in Figure 10. After undergoing bond fission, the peroxide radicals perform hydrogen abstraction to produce a midchain radical. This midchain radical then can undergo β-scission to produce two chains, one with an olefinic end group and the other with an end-chain radical. This end-chain radical can then repeat the cycle by performing another hydrogen abstraction. The cycle is terminated by either radical recombination or disproportionation. However, the rate of hydrogen abstraction and β-scission is much faster than the rate of termination due to the small concentration of radicals produced from the initial bond fission step. Termination is proportional

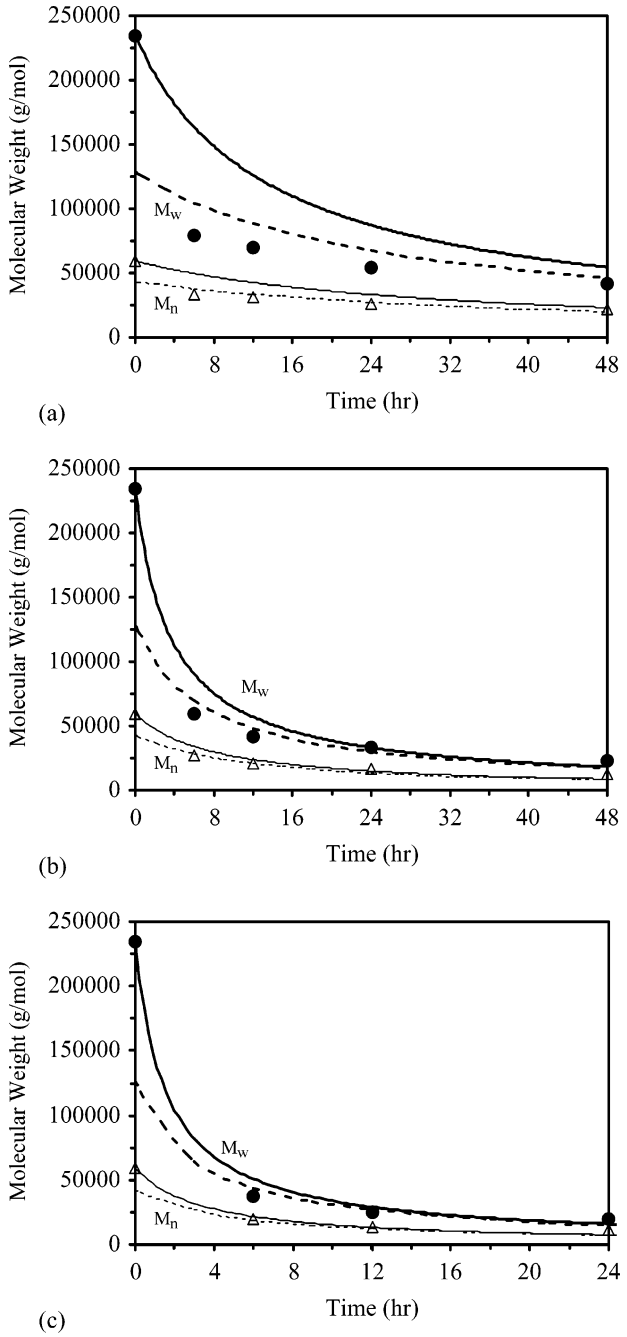

Figure 11. Comparison of model results to experimental molecular weight data in the literature[3] for the pyrolysis of polypropylene (M_n = 59 300 g/mol; M_w = 234 000 g/mol) at (a) 300, (b) 315, and (c) 325 °C for no weak links included in the model and peroxide weak links included. The solid lines represent the model results without weak links and the dotted lines represent the model results with weak links included. All the model results with weak links included overlap the *y*-axis during the beginning of the pyrolysis.

to the square of the radical concentration, while hydrogen abstraction and β-scission are proportional to the radical concentration. Therefore, the fission of each weak link on average results in the breakage of 70 polymer chains as the cycle in Figure 10 is repeated many times until termination occurs.

In Figure 11, the model results are compared to experimental data collected by Chan and Balke for the pyrolysis of polypropylene at 300, 315, and 325 °C. The model was solved with weak links included (using the same initial amount determined from the analysis of

the 275 °C data) and without weak links in the initial polymer. As is evident from Figure 11, the model results predict the data very well with weak links included in the model. However, the difference between the model results with and without weak links decreases as the temperature rises. At 325 °C, the model results with no weak links compare fairly well with the experimental data. At temperatures above 350 °C (results not shown), the differences between the model results with and without weak links become negligible after a short period of time.

At higher temperatures, the fission of carbon−carbon bonds dominates the initiation process even when weak links are included in the model. This is due to the greater sensitivity to temperature for the carbon−carbon bond fission process (bond strength 79.7 kcal/mol compared to 37.0 kcal/mol for peroxide bonds). Thus, as the temperature increases, the bond fission rate for carbon−carbon bonds increases rapidly compared to the fission rate of peroxide bonds. At high enough temperatures (>350 °C), the increase in the carbon−carbon bond fission rate coupled with the fact that carbon−carbon bonds dominate the initial polymer structure results in the carbon−carbon fission process becoming the dominant initiation mechanism. This explains why Chan and Balke found a lower overall activation energy for the pyrolysis of polypropylene in the temperature range of 275−325 °C compared to other researchers in the literature who investigated polypropylene pyrolysis at higher temperatures. In their low-temperature range, bond fission of peroxide bonds dominates initiation of the degradation of polypropylene and is the primary reason for the decrease in the polypropylene molecular weight. At temperatures above 350 °C, the fission of carbon−carbon bonds dominates the polypropylene pyrolysis mechanism even with weak links present.

Conclusions

The pyrolysis of polypropylene was modeled at the mechanistic level. The conversion among species was described using typical free radical reaction types, including intermolecular hydrogen abstraction, mid-chain β-scission, end-chain β-scission, intramolecular hydrogen transfer, radical addition, bond fission, radical recombination, and disproportionation. It was shown that allowing up to two 1,3-, 1,4-, and 1,5-intramolecular hydrogen transfers was critical to being able to capture the yields of low molecular weight products. Although 1,7- and higher intramolecular hydrogen transfers have been proposed by other researchers as main routes to low molecular weight products, they were not included in our model as they were shown to be unlikely in other literature reports and including them failed to predict key major products quantitatively. The model included over 24 000 reactions and tracked 213 species. These 213 species consisted of polymeric species with different numbers and positions of double bonds, different groups of polymeric radicals, low molecular weight radicals, and 27 that were quantified experimentally in the C1−C15 size range.

The model predictions for the evolution of the yields of the five major alkenes and the five major alkanes compare well with experimental data obtained in our laboratory for the pyrolysis of polypropylene over a temperature range of 350−420 °C. The model results for these main products were almost always within a factor of 1.5 of the experimental yields. The model was also able to capture literature data that highlighted the effect weak links have on the evolution of the polypropylene molecular weight distribution by modeling the weak links as peroxide bonds. It was shown that incorporating one peroxide bond per 180 chains resulted in the fission of 38% of the polymer chains during the initial stages of the pyrolysis process. However, at temperatures above 350 °C, the fission of carbon−carbon bonds dominates the polypropylene pyrolysis mechanism even with a small concentration of peroxide bonds present initially.

Acknowledgment. This work was supported by the MRSEC program of the National Science Foundation (DMR-0076097) at the Materials Research Center of Northwestern University and the CAREER Program of the National Science Foundation (CTS-9623741). Funding was also provided through a National Science Foundation Fellowship (Todd M. Kruse).

References and Notes

(1) De Witt, M. J.; Dooling, D. J.; Broadbelt, L. J. *Ind. Eng. Chem. Res.* **1999**, *39*, 2228−2237.
(2) Kruse, T. M.; Woo, O. S.; Wong, H.-W.; Khan, S. S.; Broadbelt, L. J. *Macromolecules* **2002**, *35*, 7830−7844.
(3) Chan, J. H.; Balke, S. T. *Polym. Degrad. Stab.* **1997**, *57*, 113−125.
(4) EPA, Office of Solid Waste Management Programs; *Municipal Solid Waste in the United States*: *2000 Facts and Figures*; U.S. EPA: Washington, DC, June 2002.
(5) Michaeli, W.; Breyer, K. *Macromol. Symp.* **1998**, *135*, 83−96.
(6) Miller, A. *Environ. Sci. Technol.* **1994**, *28*, 16A.
(7) Day, M.; Cooney, J. D.; Klein, C.; Fox, J. *Polym. Prepr.* (*Am. Chem. Soc., Div. Polym. Chem.*) **1993**, *34*, 123−124.
(8) Fouhy, K.; Kim, I.; Moore, S.; Culp, E. *Chem. Eng.* **1993**, *100*, 30−33.
(9) Scott, D. S.; Majerski, P.; Piskorz, J.; Radlein, D.; Barnickel, M. *Can. J. Chem. Eng.* **1999**, *77*, 1021−1027.
(10) Aguado, J.; Serrano, D. *Feedstock Recycling of Plastic Wastes*; The Royal Society of Chemistry: Cambridge, U.K., 1999.
(11) Wang, M.; Smith, J. M.; McCoy, B. J. *AIChE J.* **1995**, *41*, 1521−1533.
(12) Madras, G.; Smith, J. M.; McCoy, B. J. *Ind. Eng. Chem. Res.* **1996**, *35*, 1795−1800.
(13) Madras, G.; Chung, G. Y.; Smith, J. M.; McCoy, B. J. *Ind. Eng. Chem. Res.* **1997**, *36*, 2019−2024.
(14) Madras, G.; Smith, J. M.; McCoy, B. J. *Polym. Degrad. Stab.* **1997**, *58*, 131−138.
(15) Madras, G.; McCoy, B. J. *AIChE J.* **1998**, *44*, 647−655.
(16) Madras, G.; McCoy, B. J. *Ind. Eng. Chem. Res.* **1999**, *38*, 352−357.
(17) McCoy, B. J. *AIChE J.* **1993**, *39*, 1827−1833.
(18) McCoy, B. J.; Wang, M. *Chem. Eng. Sci.* **1994**, *49*, 3773−3785.
(19) McCoy, B. J.; Madras, G. *AIChE J.* **1997**, *43*, 802−810.
(20) Sezgi, N. A.; Cha, W. S.; Smith, J. M.; McCoy, B. J. *Ind. Eng. Chem. Res.* **1998**, *37*, 2582−2591.
(21) Kruse, T. M.; Woo, O. S.; Broadbelt, L. J. *Chem. Eng. Sci.* **2001**, *56*, 971−979.
(22) Wong, H.-W.; Broadbelt, L. J. *Ind. Eng. Chem. Res.* **2001**, *40*, 4716−4723.
(23) Tsuchiya, Y.; Sumi, K. *J. Polym. Sci.*: *Part A-1* **1969**, *7*, 1599−1607.
(24) Madorsky, S. L.; Straus, S. *J. Res. Natl. Bur. Stand.* **1954**, *53*, 361−370.
(25) Sousa Pessoa De Amorim, M. T.; Comel, C.; Vermande, P. *J. Anal. Appl. Pyrolysis* **1982**, *4*, 73−81.
(26) Sousa Pessoa De Amorim, M. T.; Bouster, C.; Veron, J. *J. Anal. Appl. Pyrolysis* **1982**, *4*, 103−115.
(27) Bockhorn, H.; Hornung, A.; Hornung, U.; Schwaller, D. *J. Anal. Appl. Pyrolysis* **1999**, *48*, 93−109.
(28) Chan, J. H.; Balke, S. T. *Polym. Degrad. Stab.* **1997**, *57*, 127−134.
(29) Pladis, P.; Kiparissides, C. *Chem. Eng. Sci.* **1998**, *53*, 3315−3333.

(30) Kruse, T. M.; Wong, H.-W.; Broadbelt, L. J. *Ind. Eng. Chem. Res.* **2003**, *42*, 2722−2735.
(31) Faravelli, T.; Pinciroli, M.; Pisano, F.; Bozzano, G.; Dente, M.; Ranzi, E. *J. Anal. Appl. Pyrolysis* **2001**, *60*, 103−121.
(32) Audisio, G.; Bajo, G. *Makromol. Chem.* **1975**, *176*, 991−998.
(33) Isaacs, N. S. *Physical Organic Chemistry*; Longman Scientific and Technical: New York, 1987.
(34) McMurry, J. *Organic Chemistry*; Brooks/Cole Publishing Co.: Monterey, CA, 1984.
(35) Lehrle, R. S.; Pattenden, C. S. *Polym. Degrad. Stab.* **1999**, *63*, 153−158.
(36) Woo, O. S.; Broadbelt, L. J. *Catal. Today* **1998**, *40*, 121−140.
(37) Evans, M. G.; Polanyi, M. *Faraday Soc., London Trans.* **1938**, *34*, 11−29.
(38) Woo, O. S. Resource Recovery of Polystyrene to Monomer Through Binary Mixture Pyrolysis and Base Catalysis. Ph.D. Dissertation; Northwestern University: Evanston, IL, 1999.
(39) Stein, S. E.; Lias, S. G.; Liebman, J. F.; Kafafi, S. A. *NIST Structures and Properties Users Guide*; U.S. Department of Commerce: National Institute of Standards and Technology, 1994 (January).
(40) Brandup, J.; Immergut, E. H.; Grulke, E. A. *Polymer Handbook*, 14th ed.; John Wiley and Sons: New York, 1999.
(41) Chien, J. C. W.; Kiang, J. K. Y. In *Stabilization and Degradation of Polymers*; Allara, D. L., Hawkins, W. L., Ed.; The American Chemical Society: Washington, DC, 1978; p 175.
(42) Cussler, E. L. *Diffusion*: *Mass Transfer in Fluid Systems*, 2nd ed.; Cambridge University Press: Cambridge, U.K., 1997.
(43) Watanebe, M.; Tsukagoshi, M.; Hirakoso, H.; Adschiri, T.; Arai, K. *AIChE J.* **2000**, *46*, 843−856.
(44) Petzold, L. R. *DASSL Differential/Algebraic System Solver*; Sandia National Laboratories: Livermore, CA, 1983.
(45) Dean, J. A. *Lange's Handbook of Chemistry*, 14th ed.; McGraw-Hill: New York, 1992.
(46) Blowers, P.; Masel, R. I. *J. Phys. Chem. A* **1999**, *103*, 7047−7054.
(47) Moad, G.; Solomon, D. H. *The Chemistry of Free Radical Polymerization*; Elsevier Science: Oxford, U.K., 1995.

MA030322Y